An Experimentally-Verified Thermal-Electrochemical Simulation Model of a 21700 Cell Using a Lumped Semi-Empirical Battery Model

by
Alireza Sarmadian[a], Yifei Yu[b], James Marco[b], Barbara Shollock[a], Francesco Restuccia[a*]

[a]Department of Engineering, King's College London, WC2R 2LS, United Kingdom.
[b]WMG, University of Warwick, Coventry, CV4 7AL, United Kingdom
*Corresponding Author, francesco.restuccia@kcl.ac.uk

ABSTRACT

This paper addresses, for the first time, lumped electrochemical-thermal coupled model requirements for the core temperature prediction of a cylindrical 21700 cell. This approach reduces the total number of necessary input parameters in comparison with fully physics-based models. A Newman P2D or a Newman simplified electrochemical model of Single Particle (SP) require approximately 40 and 20 parameters. By contrast, the lumped semi-empirical electrochemical-thermal model approach uses 3 fitting and 10 input parameters, simplifying the detailed knowledge required and also enabling the reduction of the load on the battery management system.

COMSOL Multiphysics has been used to achieve a coupled electrochemical-thermal model which is both accurate and with fast response (computation time: ~18 seconds) in the prediction of 21700 NMC/Si-Graphite cell potentials and core temperatures. The fitting parameters of dimensionless charge exchange, the ohmic overpotential at 1C, and the diffusion time for the calibrated model were obtained using the experimental battery data at 1C. The model is validated against a different set of data for discharge tests at 0.3 and 0.7 C-rates. These include experimental cell potential curves and core temperature measurements by using a fibre optic sensing system. Results showed that the standard deviations obtained for the cell voltage and the core temperature are respectively 0.12 V and 0.8 K.

INTRODUCTION

The thermal characteristics of lithium-ion batteries during charge and discharge are important in a variety of applications. In aerospace and automotive applications for example, thermal management of battery packs [1], battery degradation [2], ageing [3] modelling, and battery management system design are all crucial. A thermal-electrochemical coupled model with core temperature prediction capabilities, rather than just surface temperature predictions as in existing models [4], plays a prominent role in battery safety, reliability, and longevity [5]. Fast modelling is important for control purposes and health monitoring.

Current electrochemical models can be classified into three categories, namely (i) fully physics-based, (ii) simplified physics-based and (iii) equivalent circuit (EC) models. The EC approach uses several simple circuit components to create an electric circuit with dynamic voltage characteristics that approximate those of an operating battery, hence acting as a black-box model. Other battery black-box modelling techniques, such as neural networks, are also available. It is feasible to create hybrid methods by combining elements from different approaches.

Newman and his collaborators developed the most extensively used physics-based lithium-ion battery model (Known as the Doyle-Fuller-Newman model [6]) to describe the behaviour of a porous electrode battery in 1993. This model is referred to as a pseudo-two-dimensional (P2D) model. This model has undergone extensive research and has proven to be an effective tool for estimating, optimising, and predicting battery performance. To set up the P2D successfully all the battery components' geometric, thermodynamic, physical, and kinetic parameters are required as inputs. This involves a thorough understanding of the properties of individual electrode, electrolyte, and separator materials, which can only be obtained by extensive testing. The accuracy of these parameters is critical to the P2D model's reliability. Because these parameters are unique to each cell design, not all parameter values are transferable from one cell design to the next [7]. Literature-based experimental data cannot be confidently used, if they come from diverse sources, because discrepancies may occur, resulting in poor predictions. As a result, one of the most difficult aspects of physics-based modelling is determining a proper set of parameters to replicate a specific battery. To allow simulation, the P2D model requires around 40 parameters.

Researchers are constantly on the lookout for an appropriate and feasible simplification technique for the P2D model, with the Single Particle (SP) model (by Haran et al. in 1998, [8]) being the most popular. The SP model ignores the unequal distribution of lithium ions' solid-phase diffuse potential in the liquid phase, allowing an active particle to represent the complete electrode. The SP model has fewer solving equations, fewer parameters (but still over 20), and higher computational efficiency than the P2D model. Thus, it has evolved into an electrochemical model that can be used in real-time systems. However, due to the simplifying of the electrochemical process, the precision of the SP model is decreased, and it is only applicable for low to moderate-rate charge and discharge conditions.

To facilitate the parameter estimation task for the battery management system (BMS) on-board, Ekström et al. (2018, [9]) suggested a lumped semi-empirical model. Their approach, which includes three lumped models of voltage losses in the cell, can accurately estimate cell potential. One linear (resistive), one nonlinear (kinetic), and one time-dependent element are included in the model, with the latter characterising the diffusive processes in the battery. This results in a model with less than 10 input parameters. It should be noted that their developed model is isothermal. However, the potential exists to couple this

electrochemical model with a thermal model and obtain transient heat transfer characteristics. The effect of temperature on the electrochemical properties, ageing, and performance of lithium-ion cells has been discussed in a review by Alipour et al. [10], suggesting the need for thermal-electrochemical models with core temperature capabilities. The existing models are, however, only validated against experimentally-measured surface temperatures of a battery cell. There is no study suggesting a thermal-electrochemical model with experimentally-verified core temperature capabilities.

In this paper, the objective is to study, for the first time, lumped thermal-electrochemical coupled model requirements for the core temperature prediction of a cylindrical 21700 cell. Experimentally-measured core temperature and open-circuit voltage (OCV) data is used to fit three corresponding lumped semi-empirical voltage loss models. In particular, use is made of three lumped fitting parameters of the dimensionless charge exchange, the ohmic overpotential at 1C, and the diffusion time in conjunction with empirical parameters of OCV vs SOC and temperature derivatives of OCV vs. SOC, to better predict the core temperature. The new model aids to improve the design and thermal management of batteries, and the design of BMS in automotive and aerospace applications.

NOMENCLATURE

C_p	specific heat (kJ/kg k)
E_{OCV}	open circuit voltage (V)
I_{cell}	applied current (A)
J_0	dimensionless charge exchange current (-)
Q_h	battery heat source (W)
$Q_{cell,0}$	battery cell capacity (C)
Q_{mix}	heat of mixing (W)
$SOC_{average}$	average state-of-charge (-)
$SOC_{cell,0}$	initial cell state-of-charge (-)
$SOC_{surface}$	surface state-of-charge (-)
T_{ref}	reference temperature (K)
V_{cell}	battery volume (m^3)
$\eta_{IR,1C}$	ohmic overpotential at 1C (V)
η_{IR}	ohmic overpotential (V)
η_{act}	activation overpotential (V)
η_{conc}	concentration overpotential (V)
d	diameter (m)
L	length (m)
k	thermal conductivity (W/m K)
T	temperature (K)
F	Faraday's constant (C/mol)
R	molar gas constant (J/mol K)
q	heat flux by conduction (W/m^2)

Greek symbols

ρ	density (kg/m^3)
σ	standard deviation (-)
τ	diffusion time constant (s)

Subscripts

can	canister
batt	battery
man	mandrel
pos	positive
sep	separator
cc	current collector
neg	negative
fit	fitting
val	validation

THERMAL-ELECTROCHEMICAL MODEL OVERVIEW AND GOVERNING EQUATIONS

Figure 1 shows a schematic view of the integrated model by coupling a 0D lumped semi-empirical cell model with a 2D axisymmetric heat transfer model. The battery cell chemistry is modelled using the lumped model, while the temperature in the battery is modelled using the heat transfer model. The produced heat source calculated by the lumped model and the average temperature obtained from the thermal model connect the two models.

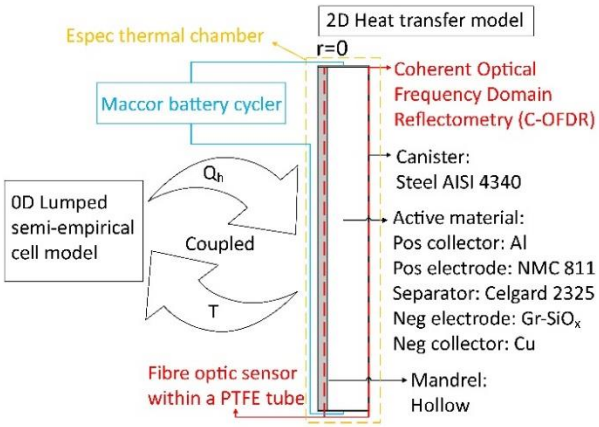

Figure 1 Schematic view of the coupled model, where the 0D lumped semi-empirical cell model provides the battery heat source to the 2D Heat transfer model, which feedbacks the temperature to the cell model.

The rationale for choosing a 0D cell model is because the heat conductivity of the components of a lithium-ion battery is rather high in comparison to the heat generated. Consequently, the battery should have a fairly consistent temperature profile in most instances. Furthermore, if modest temperature variations have minimal effect on the battery chemistry, characterising the battery chemistry using a global lumped model which is based on the battery's average temperature loses little detail. However, when there is a substantial range in temperature throughout the active battery material, a local lumped model can be employed since it is necessary to incorporate local values of the produced heat source in the thermal model. The heat transfer interface is used by the local lumped model to obtain the local temperature in the active material domain, and in return the generated heat source is provided by local lumped model to the heat transfer interface.

The battery cell voltage, E_{cell}, can be obtained based on [9] as follows:

$$E_{cell} = E_{OCV}(SOC, T) + \eta_{IR} + \eta_{act} + \eta_{conc} \quad (1)$$

where the open circuit voltage, $E_{OCV}(SOC, T)$, which is

temperature, T, and SOC dependent, is evaluated as (based on COMSOL Multiphysics® [11]):

$$E_{OCV}(SOC,T) = E_{OCV,ref}(SOC) + \left(T - T_{ref}\right)\frac{\partial E_{OCV}(SOC)}{\partial T} \quad (2)$$

where $E_{OCV,ref}(SOC)$ is open circuit voltage at a reference temperature T_{ref}, and $\frac{\partial E_{OCV}(SOC)}{\partial T}$ is the temperature derivative of the open circuit voltage versus SOC. η_{IR}, η_{act}, and η_{conc} are respectively lumped overpotentials of ohmic, activation, and concentration. Lumped voltage loss associated with ohmic processes in the electrolyte and electrodes can be obtained using

$$\eta_{IR} = \eta_{IR,1C}\frac{I_{cell}}{I_{1C}} \quad (3)$$

$$I_{1C} = \frac{Q_{cell,0}}{3600[s]} \quad (4)$$

where $\eta_{IR,1C}$ is ohmic overpotential at 1C (a fitting parameter), I_{cell} is applied current, and I_{1C} is charge at 1C. Lumped voltage loss associated with activation overpotential on both the positive and negative electrode surfaces (due to charge transfer processes) is obtained from [9] using Butler-Volmer equation [12]:

$$\eta_{act} = \frac{2RT}{F}asinh\left(\frac{I_{cell}}{2J_0 I_{1C}}\right) \quad (5)$$

where J_0 is dimensionless charge exchange current (a fitting parameter), R is the molar gas constant, and F is Faraday's constant. The equation for the lumped voltage loss associated with concentration overpotential, based on diffusion in an idealized particle, is as follows (based on [11]):

$$\eta_{conc} = E_{OCV}\left(SOC_{surface},T\right) - E_{OCV}\left(SOC_{average},T\right) \quad (6)$$

where $SOC_{average}$ and $SOC_{surface}$ are average and surface state-of-charges of the particles which are obtained using Fickian diffusion equation [13] as follows:

$$\tau\frac{\partial SOC}{\partial t} = -\nabla.(-\nabla \mathrm{SOC}) \quad (7)$$

where τ is the diffusion time constant (the third fitting parameter). The diffusion equation is solved in a 1D pseudo additional dimension corresponding to the particle dimension (an interval of length 1 with X as the dimensionless spatial variable). Depending on whether the particles are supposed to be flakes, rods, or spheres, the gradient is calculated in Cartesian, cylindrical, or spherical coordinates. The boundary conditions ($X = 0$ represents centre of the particle, $X = 1$, points at the particle surface) are:

$$\nabla SOC = 0|_{X=0} \text{ and } \nabla SOC = \frac{\tau I_{cell}}{N_{shape}Q_{cell,0}}|_{X=1} \quad (8)$$

where N_{shape} is 1 for Cartesian, 2 for cylindrical, and 3 for spherical coordinates. The initial state of charge is $SOC_{cell,0}$. Therefore, $SOC_{surface}$, is defined at the particle surface. $SOC_{average}$, is defined by integrating over the volume of the particle in the form of:

$$SOC_{average} = \frac{\int_0^1 SOC4\pi X^2 dX}{\int_0^1 4\pi X^2 dX} = 3\int_0^1 SOCX^2 dX \quad (9)$$

Finally, the electrochemical heat source required for the thermal model can be formulated (according to [11]) as follows:

$$Q_h = \left(\eta_{IR} + \eta_{act} + T\frac{\partial E_{OCV}(SOC_{surface},T)}{\partial T}\right)I_{cell} + Q_{mix} \quad (10)$$

where Q_{mix} is the heat of mixing according to [11]:

$$Q_{mix} = \frac{N_{shape}Q_{cell,0}}{\tau}\int_0^1 \frac{\partial E_{OCV,therm}}{\partial SOC}\frac{\partial SOC}{\partial X}\frac{\partial SOC}{\partial X}X^{N_{shape}-1}\partial X \quad (11)$$

and $E_{OCV,therm}$ is the thermoneutral voltage as bellow:

$$E_{OCV,therm} = E_{OCV,ref}(SOC) - T_{ref}\frac{\partial E_{OCV}(SOC)}{\partial T} \quad (12)$$

As can be seen in **Figure 1**, the 2D heat transfer model uses the geometry and materials of a 21,700-type cylindrical cell. This includes the isolator mandrel, active material consisting of two current collectors, two electrodes, and one separator as well as a canister. Active material here is in fact spirally wound layers around the mandrel that are generally tens of micrometres thick in the normal direction but tens of centimetres long in the sheet direction. In other words, instead of simulating heat conduction in each layer of the wound sheets in the radial direction (for example, each negative electrode layer, each separator layer, and so on), the wound sheets are represented as one active battery material domain. It has been proven by Gomadam et al. [14] that heat conduction in the spiral direction can be ignored in this form of spirally wound battery. This justifies using axial symmetry. The thermal conductivities are anisotropic, with a larger thermal conductivity along the battery sheets (i.e. in the cylinder length direction) than in the normal direction to the sheets (i.e. in the radial direction). The thermal conductivity in the radial direction, thermal conductivity in the cylinder length direction (based on [15]), the density, and the heat capacity (taken from [11]) of the active material can be calculated according to following equations:

$$k_r = \frac{\sum L_i}{\sum L_i/k_i} \quad (13)$$

$$k_{ang} = \frac{\sum L_i k_i}{\sum L_i} \quad (14)$$

$$\rho_{batt} = \frac{\sum L_i \rho_i}{\sum L_i} \quad (15)$$

$$C_{p,batt} = \frac{\sum L_i C_{p,i}}{\sum L_i} \quad (16)$$

where L_i is the thicknesses of the cell's several layers. k_i, ρ_i, and $C_{p,i}$ are respectively thermal conductivities, densities and heat capacities of the materials that make up these layers. Finally, heat transfer in solids (i.e., the active material, the hollow mandrel, and the canister) can be calculated numerically using energy conservation equation in the simplified form of:

$$\rho C_p\frac{\partial T}{\partial t} + \nabla.q = {Q_h}/{V_{cell}} \quad (17)$$

where q is the heat flux by conduction, and V_{cell} is the battery volume.

MODEL REQUIREMETNS: EXPERIMENTAL MEASUREMENTS AND INPUT PARAMETER VALUES

Single discharge processes at three various C rates of 0.3, 0.7 and 1C were simulated to validate the above-mentioned model. The calculations are based on a commercial high-energy 21700 battery with a rated discharge capacity of 5 Ah at 1C. The cut-off voltages for discharge and charge are 2.5 V and 4.2 V, respectively, and the nominal voltage is 3.63 V. **Figure 2** shows the surface temperature measurements used as the boundary conditions at the canister for the thermal model. The measurements are taken with a constant current (CC) discharge (using a Maccor cycler) for three C-rates of 0.3, 0.7, and 1 and by using the fibre optic sensors placed at the cell surface and core (also shown in **Figure 1**). To monitor surface and core temperature measurements, Coherent Optical Frequency Domain Reflectometry (C-OFDR), a sort of Rayleigh scattering based distributed fibre optic sensor (DFOS), is used (as

explained by Yu et al. in [16]). The system was placed within an Espec thermal chamber to maintain a constant reference (as well as ambient) temperature of 298.15 K. Temperature sensor calibration using a platinum resistance thermometer (PRT) (with an accuracy of ±0.15 K) resulted in a standard deviation of 0.27 K [16]. As was expected, the higher C-rate generated a higher temperature increase. It should be noted that, for all the curves, the temperature drops near the cut-off voltage of 2.5 V and before the current is set to zero.

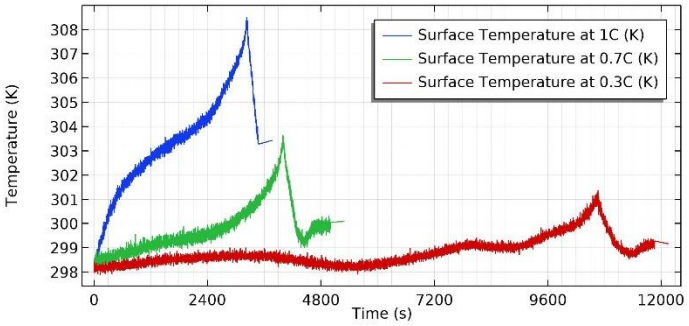

Figure 2 Surface temperature data at different C-rates of 0.3, 0.7, and 1 used as boundary conditions in the model

Table 1 Input parameters and values used in the model.

Symbol	Description	value
d_{can}	Thickness of battery canister	0.25 (mm)
r_{batt}	Battery radius	10.5 (mm)
h_{batt}	Battery height	70 (mm)
r_{man}	Hollow mandrel radius	2 (mm)
L_{neg}	Length of negative electrode	85.2 (μm) [7]
L_{sep}	Length of separator	12 (μm) [7]
L_{pos}	Length of positive electrode	75.6 (μm) [7]
$L_{neg,cc}$	Negative current collector thickness	12 (μm) [7]
$L_{pos,cc}$	Positive current collector thickness	16 (μm) [7]
kT_{pos}	Positive electrode thermal conductivity	1.58 (W/m.K)
kT_{neg}	Negative electrode thermal conductivity	1.04 (W/m.K)
$kT_{neg,cc}$	Negative current collector thermal conductivity	398 (W/m.K)
kT_{sep}	Separator thermal conductivity	0.344 (W/m.K)
ρ_{pos}	Positive electrode density	4870 (kg/m^3) [7]
ρ_{neg}	Negative electrode density	2300 (kg/m^3) [7]
$\rho_{pos,cc}$	Positive current collector density	2770 (kg/m^3)
$\rho_{neg,cc}$	Negative current collector density	8933 (kg/m^3)
ρ_{sep}	Separator density	1009 (kg/m^3)
$C_{p,pos}$	Positive electrode heat capacity	840.1 (J/kg·K)
$C_{p,neg}$	Negative electrode heat capacity	1437.4 (J/kg·K)
$C_{p,pos,cc}$	Positive current collector heat capacity	875 (J/kg·K)
$C_{p,neg,cc}$	Negative current collector heat capacity	385 (J/kg·K)
$C_{p,sep}$	Separator heat capacity	1978.2 (J/kg·K)
T_{inlet}	Inlet temperature	298.15 (K)
T_{init}	Initial temperature	298.15 (K)
Q_{batt}	Cell capacity	5 (Ah) [7]
$\eta_{IR,1C}$	Ohmic overpotential at 1C	4.5 (mV)
J_0	Dimensionless charge exchange current	0.85 (-)
τ	Diffusion time constant	1000 (s)

Table 1 lists the input parameters and values associated with the cell geometry, thermophysical, and material properties as well as initial values used in the model. The initial values of ohmic overpotential at 1C, $\eta_{IR,1C}$, dimensionless charge exchange current, J_0, and diffusion time constant, τ are obtained from a sweep study of prepared model. These initial values were used in the curve fitting to calibrate the model. As most of the input parameter values are not available in the datasheet of LGM50 21700 5Ah cell, the values are taken from an empirical study by Warwick Manufacturing Group (WMG) on the cell parameterisation of this cell [7]. The positive electrode is $LiNi_{0.8}Mn_{0.1}Co_{0.1}O_2$ and the negative electrode is graphite-SiO_x. For a few cases, the values are estimated based on existing information in literature.

RESULTS AND DISCUSSION

Commercial software, COMSOL Multiphysics® version 5.6, was used to carry out numerical simulations. The solution was obtained using MUMPS direct time-dependent solver. To calibrate the model, the parameter fitting is performed only for the load data set containing discharge at 1C. The fitting parameters of ohmic overpotential at 1C, dimensionless charge exchange density, and diffusion time were obtained by employing nonlinear least square regression (global least-square objective was set for the cell potential) using the Levenberg-Marquardt algorithm.

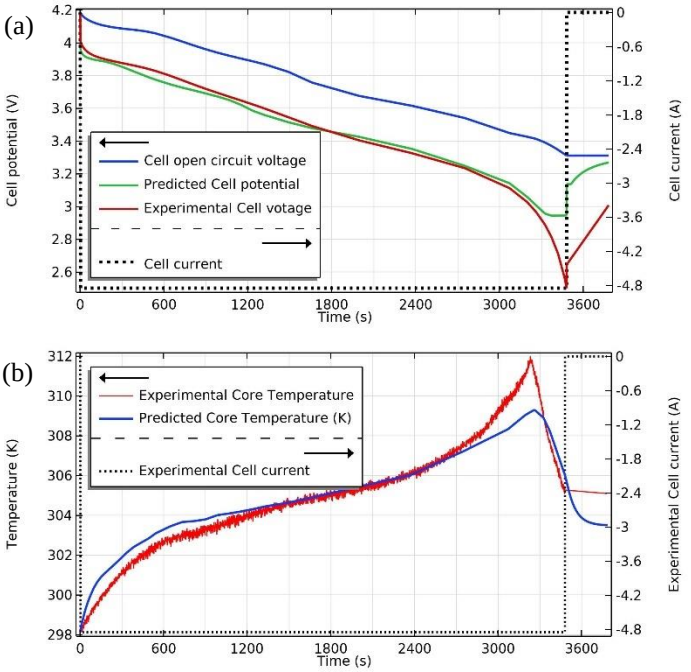

Figure 3 Results associated with the calibrated model at 1 C-rate: a) the predicted cell potential versus the experimental voltage for the shown constant current discharge and OCV, and b) the predicted temperature against the measurements.

Figure 3 shows the predicted cell potential (Fig 3a) and core temperature (Fig 3b) at 1C against the associated experimental measurements. The achieved fitting parameter values are $\eta_{IR,1C} = 80\ mV$, $J_0 = 0.11$, and $\tau = 5500\ s$. To achieve better

fitting accuracies, the lumped battery model requires input parameters of the $E_{OCV,ref}(SOC)$ and $\frac{\partial E_{OCV}(SOC)}{\partial T}$ in equations (1) and (2), respectively. For this, experimental results for 1C are used. The temperature derivatives of the open circuit voltage are obtained using different difference schemes of first and second order. However, when all the schemes were compared, a 2 per cent enhancement in the accuracy of the cell potential standard deviation was achieved by using a second-order forward difference scheme as follows:

$\frac{\partial E_{OCV}(SOC)}{\partial T} \approx \frac{E_{OCV,i+2}-4E_{OCV,i-1}+3E_{OCV,i}}{2\delta T}$, 2nd order forward (18)

Table 2 shows the results of a mesh independence study that compared the maximum core temperatures at different discharge C-rates (with the same fitting parameters) with total grid numbers of 48, 174, and 468. The associated total number of DOFs solved are included. As can be seen, for all C-rates, the variation in maximum core temperature between mesh counts of 178 and 468 is negligible. The converged element count was chosen to correspond to the lowest mesh count which gave a maximum absolute temperature-change of less than 0.1%. Therefore, the mesh count of 468 satisfies this criterion for three C-rates. It is noteworthy that the mesh convergence for the case at 1 C-rate is met for a mesh count of 174.

Table 2 Maximum core temperature vs. grid element count.

Discharge C-rate	Max predicted core temperatures (K) and Number of DOFs solved for (N. DOFs) **Fitting par.**: $\eta_{IR,1C} = 80\ mV, J_0 = 0.11$, and $\tau = 5500\ s$		
	Element count:48 N. DOFs:236	Element count:174 N. DOFs:778	Element count:468 N. DOFs:2006
1 C	309.63	309.38	309.30
0.7 C	303.22	303.60	303.58
0.3 C	301.08	300.10	300.37

Table 3 represents the cell voltage and core temperature standard deviations as well as computational time for all the mesh counts. Each simulation takes between 5 and 18 seconds (depending on the mesh counts) by using an Intel® Xeron® Gold 6226R (2.90GHz) processor and 64 GB RAM. To check the generalisation of the model, the fitting parameters found for the 1 C-rate data were attempted in the simulation of the discharge cases of 0.7 and 0.3 C-rates. To make room for inspection, two standard deviations of fitting, σ_{fitt}, and validation, σ_{val}, are defined in **Table 3**. σ_{fitt} indicates the calculated standard deviations for the fitting process of 1 C-rate data set, and σ_{val}, represents the standard deviations of the validation data set of 0.7 and 0.3 C-rates. For 468 mesh elements simulation, the core temperature and cell voltage standard deviations at 1C (i.e. fitting) are respectively 0.7866 K and 0.1199 V.

Table 3 Standard deviations for core temperature and cell potential vs. grid element count.

Standard deviation of:	C-rate	Standard deviations (fitting at 1 C-rate and validation at 0.3 and 0.7 C-rates) for core temperature (K), cell potential (V), and computational time (CT) **($\eta_{IR,1C} = 80\ mV, J_0 = 0.11$, and $\tau = 5500\ s$)**		
		Mesh elements 48, CT=5s	Mesh elements 174, CT=8s	Mesh elements 468, CT=18s
σ_{fitt}	1 C	0.7972, 0.1199	0.8043, 0.1197	0.7866, 0.1199
σ_{val}	0.7 C	0.3714, 0.1171	0.3140, 0.1139	0.3123, 0.1139
σ_{val}	0.3 C	0.2873, 0.0981	0.2784, 0.0965	0.2724, 0.0969

Figure 4 and **Figure 5** show the validation results for the cell potential and the core temperature simulations respectively at 0.7 and 0.3 C-rates. As can be seen, the calibrated model for fitting parameters at 1C was successfully used in the prediction of load and temperature curves at 0.7 and 0.3 C-rates, which offers strong generalisation. By contrast, in a calibrated P2D model for the same commercial cell by Chen et al [7], different diffusion coefficient values were set when the C-rates in the simulations varied. In terms of accuracy, the RMS errors reported by Chen et al. [7] are however better which is as a result of using the high-fidelity P2D model (P2D RMSE: 46 mV and the current lumped model RMSE: 100 mV). The simulation times, however, are not reported in their work. In another recent study by O'Regan et al. [17], a DFN cell model is coupled with a 0D thermal model to predict the surface temperatures of an M50 21700 cell (not the core temperature). It is reported that the simulations take between 10 and 20 minutes (between 33 and 240 times longer than the lumped model simulations here). Furthermore, the achieved cell voltage RMSE is 0.14 V when the Chen et al. [7] parameter set is used and 0.10 V for O'Regan et al. [17] updated parameter set. This is similar to the aforementioned RMSE of 100 mV for the lumped model in this study. O'Regan et al. [17] have not reported the RMSE or standard deviations for their surface temperature predictions. By inspecting the provided results, however, the standard deviations in [17] should be similar to the lumped model standard deviations in **Table 3**.

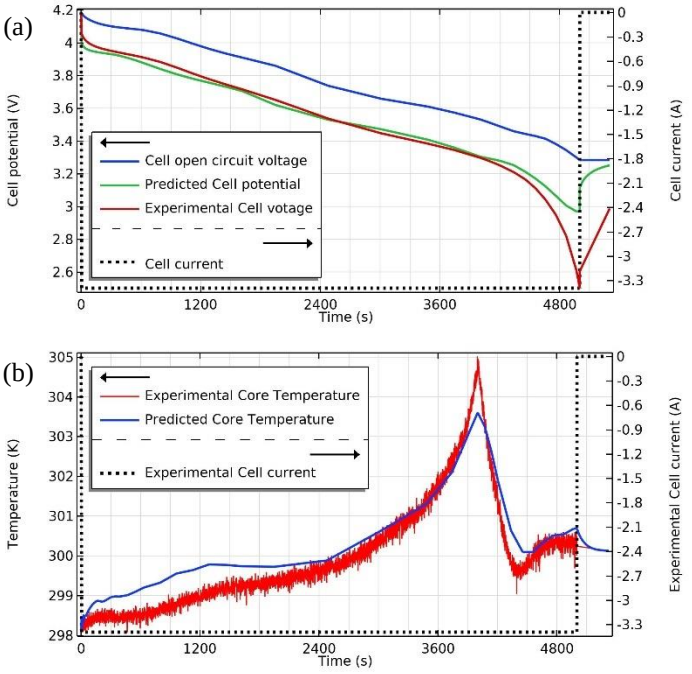

Figure 4 Validation results when the model is tested for the data at 0.7 C-rate against the experimental measurements: a) the predicted cell potential voltage for the shown constant current discharge and OCV, and b) the predicted temperature. Peak times are closely aligned.

As can be seen in **Table 3**, the core temperature and cell voltage standard deviations at 0.7C are 0.3123 K and 0.1139 V.

The associated standard deviations at 0.3 are 0.2724 K and 0.0969 V. There are reductions in the standard deviations from 1C to 0.3C. These reductions are due to the smaller temperature gradients in the experimental data points of the lower C-rate results. Furthermore, there are more experimental data points (higher resolution) for lower C-rates considering the fixed sample rate. The high prediction accuracy along with the fast computational time of the calibrated model here, therefore, offer potentially promising applications to future model-based thermal management systems.

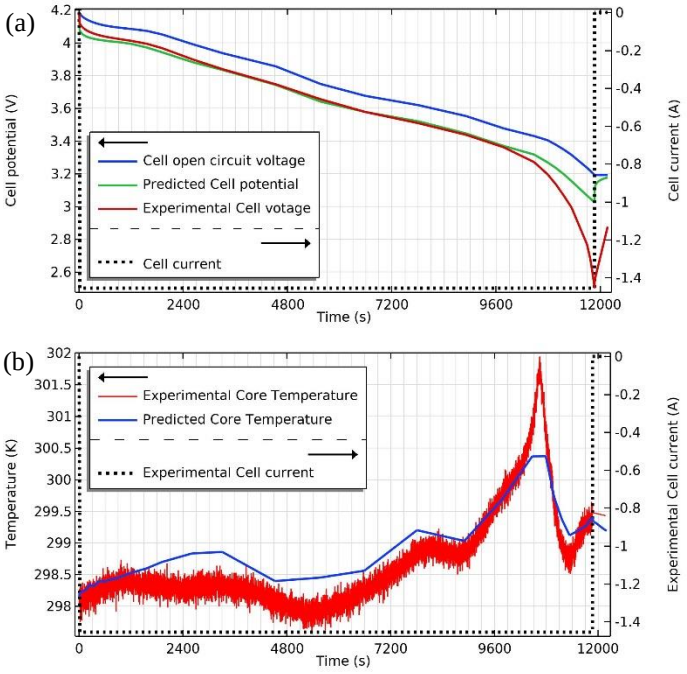

Figure 5 Validation results when the model is tested for the data at 0.3 C-rate against the experimental measurements: a) the predicted cell potential voltage for the shown constant current discharge and OCV, and b) the predicted temperature.

CONCLUSIONS

Numerical simulations have been undertaken to investigate, for the first time, the model requirements of a thermal-electrochemical model of a high-energy 2170 cell with core temperature prediction capabilities. In this regard, a 0D lumped semi-empirical cell model is coupled with a 2D axisymmetric thermal model. An experimental data set containing a range of C-rates (i.e. 0.3, 0.7 and 1) during constant current discharge of the cell has been used for calibration and validation of the model. The cell is instrumented with a fibre sensing sensor to measure the surface and core temperatures. The surface temperature measurements at the canister are used as boundary conditions for the thermal model, and the experimental OCV data are used as inputs to the lumped model. The parameter fitting is conducted to calibrate the model using only the experimental results at 1C. Then, it is validated against a different set of data for measurements at 0.7 and 0.3 C-rates. The fitting and validation standard deviations for cell voltages and core temperatures as well as the computational time are fully defined. The main conclusions are:

- The calibrated model at 1C showed strong generalisation for the constant current discharges at 0.3 and 0.7 C-rates. The existing high-fidelity models of P2D in the literature have better RMSEs for cell potential but do not offer such generalisation.
- The developed model predicts the cell potential and core temperature results within 18 seconds. That is between 33 and 240 times faster than computational times reported in the literature for a calibrated model of a similar commercial cell (which only predicts surface temperature).

ACKNOWLEDGEMENTS

The authors wish to acknowledge funding support for this project from the EPSRC Prosperity Partnership with Jaguar Land Rover (JLR), project EP/R004927/1.

References

[1] W. Zhuang, Z. Liu, H. Su, G. Chen, An intelligent thermal management system for optimized lithium-ion battery pack, Applied Thermal Engineering, 189 (2021) 116767.

[2] A. Thingvad, L. Calearo, P.B. Andersen, M. Marinelli, Empirical Capacity Measurements of Electric Vehicles Subject to Battery Degradation from V2G Services, IEEE Transactions on Vehicular Technology, 70 (2021) 7547-7557.

[3] D. Šeruga, A. Gosar, C.A. Sweeney, J. Jaguemont, J. Van Mierlo, M. Nagode, Continuous modelling of cyclic ageing for lithium-ion batteries, Energy, 215 (2021) 119079.

[4] D. Li, L. Yang, C. Li, Control-oriented thermal-electrochemical modeling and validation of large size prismatic lithium battery for commercial applications, Energy, 214 (2021) 119057.

[5] P.G. Anselma, P. Kollmeyer, J. Lempert, Z. Zhao, G. Belingardi, A. Emadi, Battery state-of-health sensitive energy management of hybrid electric vehicles: Lifetime prediction and ageing experimental validation, Applied Energy, 285 (2021) 116440.

[6] M. Doyle, T.F. Fuller, J. Newman, Modeling of galvanostatic charge and discharge of the lithium/polymer/insertion cell, Journal of The Electrochemical Society, 140 (1993) 1526.

[7] C.-H. Chen, F.B. Planella, K. O'regan, D. Gastol, W.D. Widanage, E. Kendrick, Development of experimental techniques for parameterization of multi-scale lithium-ion battery models, Journal of The Electrochemical Society, 167 (2020) 080534.

[8] B.S. Haran, B.N. Popov, R.E. White, Determination of the hydrogen diffusion coefficient in metal hydrides by impedance spectroscopy, Journal of Power Sources, 75 (1998) 56-63.

[9] H. Ekström, B. Fridholm, G. Lindbergh, Comparison of lumped diffusion models for voltage prediction of a lithium-ion battery cell during dynamic loads, Journal of Power Sources, 402 (2018) 296-300.

[10] M. Alipour, C. Ziebert, F.V. Conte, R. Kizilel, A review on temperature-dependent electrochemical properties, aging, and performance of lithium-ion cells, Batteries, 6 (2020) 35.

[11] C. Multiphysics®v.5.6, Battery Design Module User's Guide, in, https://doc.comsol.com/5.6/doc/com.comsol.help.battery/BatteryDesignModuleUsersGuide.pdf, © 1998–2020 COMSOL, pp. 309-311.

[12] E.J. Dickinson, A.J. Wain, The Butler-Volmer equation in electrochemical theory: Origins, value, and practical application, Journal of Electroanalytical Chemistry, 872 (2020) 114145.

[13] K.E. Thomas, J. Newman, R.M. Darling, Mathematical modeling of lithium batteries, in: Advances in lithium-ion batteries, Springer, 2002, pp. 345-392.

[14] P.M. Gomadam, R.E. White, J.W. Weidner, Modeling heat conduction in spiral geometries, Journal of The Electrochemical Society, 150 (2003) A1339.

[15] S.-C. Chen, Y.-Y. Wang, C.-C. Wan, Thermal analysis of spirally wound lithium batteries, Journal of The Electrochemical Society, 153 (2006) A637.
[16] Y. Yu, T. Vincent, J. Sansom, D. Greenwood, J. Marco, Distributed internal thermal monitoring of lithium ion batteries with fibre sensors, Journal of Energy Storage, 50 (2022) 104291.
[17] K. O'Regan, F.B. Planella, W.D. Widanage, E. Kendrick, Thermal-electrochemical parameters of a high energy lithium-ion cylindrical battery, (2022).